



# *mdm2* gene amplification is associated with luminal breast cancer progression in humanized PDX mice and a worse outcome of estrogen receptor positive disease

Anja Kathrin Wege<sup>1</sup> | Eva-Maria Rom-Jurek<sup>1</sup> | Paul Jank<sup>2</sup> | Carsten Denkert<sup>2</sup> | Peter Ugocsai<sup>1</sup> | Christine Solbach<sup>3</sup> | Jens-Uwe Blohmer<sup>4</sup> | Bruno Sinn<sup>4</sup> | Marion van Mackelenbergh<sup>5</sup> | Volker Möbus<sup>6</sup> | Andreas Trumpp<sup>7</sup> | Elisabetta Marangoni<sup>8</sup> | Nicole Pfarr<sup>9</sup> | Christoph Irlbeck<sup>10,11</sup> | Jens Warfsmann<sup>10,11</sup> | Bernhard Polzer<sup>10,11</sup>  | Florian Weber<sup>12</sup> | Olaf Ortmann<sup>1</sup> | Sibylle Loibl<sup>13</sup> | Valentina Vladimirova<sup>13</sup> | Gero Brockhoff<sup>1</sup> 

<sup>1</sup>Department of Gynecology and Obstetrics, University Medical Center Regensburg, Regensburg, Germany

<sup>2</sup>Institute of Pathology, Philipps-University Marburg, UKGM University Hospital Marburg, Marburg, Germany

<sup>3</sup>Department of Gynecology and Obstetrics, University Hospital Frankfurt, Frankfurt, Germany

<sup>4</sup>Breast Cancer Center, Charité Universitätsmedizin Berlin, Berlin, Germany

<sup>5</sup>Department of Gynecology and Obstetrics, Schleswig-Holstein University Hospital, Kiel, Germany

<sup>6</sup>Department of Medicine II, Hematology and Oncology, Goethe University of Frankfurt, Frankfurt, Germany

<sup>7</sup>Division of Stem Cells and Cancer, German Cancer Research Center (DKFZ) and DKFZ-ZMBH Alliance, Institute for Stem Cell Technology and Experimental Medicine (HI-STEM gGmbH), German Cancer Consortium (DKTK), Heidelberg, Germany

<sup>8</sup>Department of Translational Research, Institute Curie, PSL Research University, Paris, France

<sup>9</sup>Institute of Pathology, Technical University Munich, Munich, Germany

<sup>10</sup>Division of Personalized Tumor Therapy, Fraunhofer Institute for Toxicology and Experimental Medicine, Regensburg, Germany

<sup>11</sup>Department of Experimental Medicine, University of Regensburg, Regensburg, Germany

<sup>12</sup>Institute of Pathology, University of Regensburg

<sup>13</sup>German Breast Group, GBG Forschungs GmbH, Neu-Isenburg, Germany

## Correspondence

Gero Brockhoff, Department of Gynecology and Obstetrics, University Medical Center Regensburg, University of Regensburg, Franz-Josef-Strauß-Allee 11, 93053 Regensburg, Germany.  
Email: gero.brockhoff@ukr.de

## Funding information

Deutsche Krebshilfe, Grant/Award Number: 111536

## Abstract

Estrogen receptor-positive breast cancer is a highly prevalent but heterogeneous disease among women. Advanced molecular stratification is required to enable individually most efficient treatments based on relevant prognostic and predictive biomarkers. First objective of our study was the hypothesis-driven discovery of biomarkers involved in tumor progression upon xenotransplantation of Luminal breast cancer into humanized mice. The second objective was the marker validation and correlation with the clinical outcome of Luminal breast cancer disease within the GeparTrio trial. An elevated *mdm2*

**Abbreviations:** BC, breast cancer; BM, bone marrow; DFS, disease free survival; ER, estrogen receptor; FISH, fluorescence in situ hybridization; hPDX, human patient derived xenotransplant; HSCs, hematopoietic stem cells; HTM, humanized tumor mice; k.d., knock-down; NSG, NOD scid gamma; OS, overall survival; TICs, tumor initiating cells; WGA, whole genome amplification.

This is an open access article under the terms of the Creative Commons Attribution-NonCommercial-NoDerivs License, which permits use and distribution in any medium, provided the original work is properly cited, the use is non-commercial and no modifications or adaptations are made.

© 2021 The Authors. *International Journal of Cancer* published by John Wiley & Sons Ltd on behalf of UICC.

gene copy number was associated with enhanced tumor growth and lung metastasis in humanized tumor mice. The viability, proliferation and migration capacity of inherently *mdm2* positive breast cancer cells in vitro were significantly reduced upon *mdm2* knock-down or anti-*mdm2* targeting. An *mdm2* gain significantly correlated with a worse DFS and OS of Luminal breast cancer patients, albeit it was also associated with an enhanced preoperative pathological response rate. We provide evidence for an enhanced Luminal breast cancer stratification based on *mdm2*. Moreover, *mdm2* can potentially be utilized as a therapeutic target in the Luminal subtype.

#### KEYWORDS

humanized tumor mice, Luminal breast cancer, *mdm2* amplification, tumor engraftment, tumor progression

#### What's new?

Breast cancer is extremely heterogeneous, even within subtypes. For best outcomes, therapies must be tailored to the molecular profile of the particular tumor. Here, the authors searched for new biomarkers in ER-positive breast cancer using a humanized tumor mouse (HTM) model, which replicates a functional human immune system. They discovered that amplification of a gene, *mdm2*, was associated with tumor progression. Treatment with agents that inhibit *mdm2* slowed down cell proliferation, viability and migration of cancer cells in vitro. Clinical testing for *mdm2* status could help improve targeted treatment for these patients.

## 1 | INTRODUCTION

Humanized tumor mice (HTM) represent a powerful animal model in cancer research to carry out treatment studies under human-like conditions. Upon xenotransplantation, either based on human cancer cell lines (HTM) or on patient-derived primary tumors (hPDX), tumor growth takes place in the presence of a functional human immune system. Lymphopoiesis and myelopoiesis occurs upon neonatal transplantation of human cord blood-derived hematopoietic stem cells (HSCs), which ensures a considerable degree of immunological tolerance against mouse tissue.<sup>1</sup> Tumor transplantation into NOD *scid* gamma (NSG) mice can be done, for example, intrahepatically, subcutaneously or orthotopically (eg, into the mammary fat pad), which has an impact on tumor cells and tissues to engraft and to maximally adapt to a species-foreign environment. Only a successful engraftment and an efficacious adaptation enable the most genuine human tumor growth and progression in mice, which is an essential basis for relevant pre-clinical treatment studies.

So called tumor initiating cells (TICs) have been found to come along with an enhanced capacity to colonize in immunodeficient mice.<sup>2</sup> The initiation of tumor engraftment and tumor growth is evidently associated with stem cell characteristics, that is, the ability of malignant cells to self-renew, to propagate and to differentiate. Although, a number of markers are known to be associated with tumor initiation and propagation, the characterization and identification of TICs with an enriched malignant potential is challenging since tumor initiating and stem cells show a dynamic physiology and varying genotypes and phenotypes in individual tumor types and subtypes.

Among solid tumors breast cancer (BC) is on the cellular and molecular level a highly heterogeneous disease.<sup>3</sup> The description of molecular portraits of humane BC about 20 years ago<sup>4</sup> led to the categorization of five major subtypes, which are mainly differentiated by their proliferation activity and the amount of hormone-receptor as well as HER2-receptor expression. The main taxonomic subtypes include so called “Luminal-A” and “B,” “Luminal-HER2-positive,” “HER2-enriched” and “triple negative” (ie, absence of hormone and HER2-receptor expression) BC.<sup>3</sup> These BC subtypes markedly differ in terms of course and outcome of disease as well as therapy options. In addition, there is a substantial heterogeneity even within individual BC categories with respect to disease progression and treatment response. For example, estrogen-receptor (ER) positive tumors represent indeed the largest BC subgroup (about 70% of all BCs) from which about 70% of all BCs are being assigned to the Luminal-A and about 30% to the Luminal-B type.<sup>5</sup> While Luminal-A typically comes with a pronounced ER expression but rather low-proliferation capacity the Luminal-B subtype is characterized by a lower ER expression, higher grading (ie, less tissue differentiation) and enhanced proliferation activity. Based on these symptomatic traits Luminal-B BC shows better response rates to cytotoxic (ie, antiproliferative) treatments while Luminal-A BC shows higher sensitivity to endocrine (ie, hormone) therapies.<sup>3,6,7</sup> Accordingly, complementing an endocrine treatment of Luminal-A BC by chemotherapy is likely to result in an overtreatment. Nevertheless, besides generally good treatment responses of Luminal BC an appreciable number relapses are seen in both groups,<sup>8</sup> but more often in Luminal-B. Thus, further stratification of Luminal BC will help to render more precisely discrete prognoses for BC patients and to identify individually most effective treatment modalities.

Moreover, an enhanced stratification will contribute to therapy de-escalation wherever possible.

In our study we generated hPDX by xenotransplantation of immunodeficient, humanized NSG mice with primary ER-positive BC tissues. We determined the engraftment efficiency and evaluated tumor growth and progression. These parameters were correlated to phenotypic and genotypic tumor characteristics. We applied immunohistochemistry and flow cytometry for tumor and immune cell characterization and used panel sequencing of BC relevant genes to identify genomic aberrations, which were potentially associated with tumor growth, dissemination and metastasis. Most strikingly, we identified a gain of mouse double minute-2 and 4 homolog (*mdm2/mdm4*) gene and/or a mutation of the TP53 locus to be associated with a higher engraftment efficiency in hPDX. Moreover, we observed an enhanced tumor progression and formation of lung metastasis in these mice bearing an *mdm2* gain. Remarkably, lung metastasis disseminated cells in the bone marrow (BM) of tumors with *mdm2* amplification were strongly associated with an elevated c-Met and CD44 expression. In vitro experiments revealed a reduced cell vitality, proliferation and migration capacity of BC cells with inherent *mdm2* amplification upon *mdm2* protein knockdown (k.d.) or *mdm2* inhibition. The assessment of *mdm2* gene copy number via fluorescence-in situ-hybridization (FISH) on ER-positive BC subcohort derived from the GeparTrio trial,<sup>9</sup> retrospectively disclosed a shortened disease free (DFS) and overall survival (OS) of BC patients who harbored an *mdm2* gain compared to those without *mdm2* alteration.

A prospective validation of *mdm2*, c-Met and CD44 as prognostic biomarkers in ER-positive BC can be considered to complement the clinicopathological diagnostics and thereby might enhance the stratification of Luminal BC. Prospectively, *mdm2* might not only serve as a prognostic, but also as a predictive marker and therapeutic target in Luminal BC, even though further systematic preclinical treatment studies in vivo are required.

## 2 | MATERIALS AND METHODS

### 2.1 | Isolation of hematopoietic stem cells from umbilical cord blood

In order to humanize mice, CD34<sup>+</sup> hematopoietic stem cells (HSC) were isolated from the umbilical cord blood based on the procedure described the first time in 2011.<sup>1</sup> More information is given in the Supporting Information Material.

### 2.2 | Tumor tissues processing for mouse transplantation

All patient-derived samples included in the study were premenopausal or postmenopausal women diagnosed with primary or metastatic BC and underwent surgery at the Department of Gynecology (University of Regensburg). Fresh, solid tumor material was removed under sterile conditions by a pathologist upon the Institute of Pathology at the (University of Regensburg). The tumor was collected in prewarmed

basal medium (DMEM/F12, 1% HEPES, 1% Pen/Strep and 1% Amphotericin B) in a petri dish and minced into fragments of 2 × 2 mm. The tumor fragments were either transplanted subsequently into NSG mice or cryopreserved.

### 2.3 | Generation of NSG based hPDX

Patient tumor samples were prepared as described above and the transplantation was carried out in 7 to 8 weeks old, virgin, non-ovariectomized, humanized female NOD.Cg-Prkdc<sup>scid</sup> Il2ry<sup>tm1Wjl</sup>/SzJ (NSG) mice according to the protocol established by Al-Hajj.<sup>10</sup> Briefly, mice were disinfected at the mammary fat pad and through a small incision, the tumor fragments were transplanted into the inguinal right fat pad and 50 µL of Matrigel (R&D Systems, Inc., Minneapolis, Minnesota) was added together with a s.c. 0.18 mg 17β-estradiol pellet (Innovative Research of America, Florida).

In addition to primary patient-derived tumor tissues three previously established patient-derived xenograft (PDX) tumors provided by Dr. Marangoni (Institute Curie, Paris, France) were sent to our laboratory (PT-S2, PT-S3 and PT-S4) and preprocessed as described above.<sup>11-14</sup> Another two PDX tumors (PT-CTC and PT-E2) were provided by Prof. Andreas Trumpp (HI-Stem, Heidelberg, Germany).<sup>2,15</sup> These mice were transplanted by s.c. neonatal transplantation of 2 × 10<sup>6</sup> tumor cells diluted in 20 µL DMEM and 10 µL Matrigel using a BD Safety Glide Insulin syringe. The PDX models were monitored for 12 months and euthanized beforehand if maximum tumor size (15 mm) was reached or any signs of sickness occurred. The previously established PDX tumors provided by the collaboration partners were not initially analyzed with respect to *mdm2*, *mdm4* or TP53 but randomly selected for our study. Just like the other successfully engrafted tumor samples used here they were retroactively subjected to panel sequencing.

### 2.4 | Flow cytometric analyses of immune cell reconstitution and tumor phenotyping from hPDX

Phenotyping of tumor and immune cells derived from hPDX was done by flow cytometry using a FACS Canto-II flow cytometer run by the Diva software v7.0 (BD Biosciences, San Jose, California) equipped with a blue (488 nm), violet (405 nm) and red (633 nm) laser excitation. Unspecific binding was blocked by incubating the cells in 1% mouse serum for 10 minutes and appropriate mouse immunoglobulin antibodies were used as isotype controls for all staining. Antibodies used for flow-cytometric analyses are specified in the Supporting Information Material.

### 2.5 | Embedding of HTM-derived tumor samples and immunohistochemistry

Tissue specimens (tumor and lung) were fixed with 4% formalin from which 1.5-µm paraffin sections were prepared. Specimens were

deparaffinized and pretreated by microwave heating for 30 minutes at 320 W in 0.1 M citrate buffer adjusted to pH 7.3. The immunostainings were automatically performed on a Ventana Nexes autostainer (Ventana, Tucson, Arizona) by using the streptavidin-biotin-peroxidase complex method and 3,3'-diaminobenzidine as chromogen. The autostainer was programmed based on the instructions given by the iView DAB detection kit (Ventana). Antibodies used for immunohistochemistry are specified in the Supporting Information Material.

## 2.6 | mdm2 knockdown and anti-mdm2 (AMG232) treatment

ZR-75-1 cells (RRID: DVCL\_0588, ATCC via LGC Standards GmbH, Wesel Germany) were incubated under standard culture conditions in RPMI-1640 medium supplemented with phenol red and 5% FCS (PAN Biotech, Aidenbach, Germany). mdm2 expression in ZR-75-1 cells was knocked down using ON TargetPlus smart pool siRNA in DharmaFECT-1T-2011-02 (Horizon Dharmacon, Lafayette, Colorado). Untreated cells and cells treated with nontargeting Pool siRNA were used as control. ZR-75-1 were seeded at a density of 400 000 cells per T25 tissue flask and cultured in RPMI-1640 medium supplemented with 5% FCS overnight. On the following day, the medium was replaced with RPMI-1640 medium supplemented with 1% FCS and the transfection was performed according to the manufacturer's protocol. On day four after transfection, the cells were either harvested with trypsin-EDTA for further experiments or lysed with 50  $\mu$ L lysis buffer (100  $\mu$ L cell lysis buffer, 10  $\mu$ L PMSF [1 mM], 10  $\mu$ L HALT protease inhibitor and 880  $\mu$ L aqua dest. for protein biochemical analysis.

For AMG232 treatment studies, ZR-75-1 were seeded at a density of 400 000 cells per T25 tissue flask and cultured in RPMI-1640 medium supplemented with 5% FCS overnight. The next day the medium was changed and the cells treated with 0.1 or 1  $\mu$ M AMG232 inhibitor (Axon Medchem BV, Groningen, The Netherlands). DMSO-treated cells and cells without treatment served as control. The cells were exposed for 48 and 72 hours to AMG232 and then harvested with trypsin-EDTA for further analyses.

ZR-75-1 cells were authenticated by short-tandem repeat profiling at the beginning of the study and within the last 3 years (DSMZ, Braunschweig, Germany). In addition, all experiments were performed with mycoplasma-free cells.

## 2.7 | Migration assay

Determination of tumor cell wound closure and migratory properties were analyzed by a wound-healing assay. In brief, 80 000 cells were seeded in each chamber of a 2-Well Culture-Insert (35 mm) (Ibidi, Gräfelting, Germany) fixed in a 6-well plate. The cells were allowed to adhere overnight. Next day the insert was removed, the cells were washed with PBS to remove cell debris and fresh medium was added

to the well. The cell scratch was visualized at 20-fold magnification by light microscopy and documented at time intervals between 6 and 216 hours after chamber removal. Closure of the scratch area was calculated by the AxioVision software (Ver. 4.4, Carl Zeiss GmbH, Göttingen, Germany).

## 2.8 | Western blotting

Western blotting was performed exactly as described recently.<sup>16</sup> A brief description of the procedure is given in the Supporting Information Material.

## 2.9 | Flow cytometric analysis of cell proliferation and cellular apoptosis

Upon harvesting by trypsinization and separation the cells were washed twice with PBS fixed and permeabilized in cooled in MeOH (70%). After overnight incubation, cells were washed twice with PBS, incubated for 20 minutes in the presence of RNAase at 37°C and finally stained with 1  $\mu$ g/mL DAPI 30 minutes prior to analysis. DNA histograms were quantified using the ModFit LT 3.2 software (Verity Software House, Topsham, Maine) upon discrimination of cell doublets, aggregates and debris via pulse processing.

For the analysis of apoptosis, adherent cells and those of the supernatant were harvested, pooled and suspended in 75  $\mu$ L Annexin-V-FITC solution containing 5  $\mu$ L Annexin-V-FITC and 70  $\mu$ L binding buffer. After 20 minutes of incubation on ice in the dark, the cells were centrifuged and resuspended in 200  $\mu$ L binding buffer. Prior to the measurement, the DAPI dye was added to a final concentration of 0.1  $\mu$ g/mL).

## 2.10 | Low pass sequencing of DTC

Single cell whole genome amplification (WGA) products were prepared for copy number variant (CNV) analysis by Ampli1 LowPass kit for Illumina (Menarini Silicon Biosystems, Pennsylvania).<sup>17</sup> Briefly, starting from purified primary Ampli1 WGA product, barcoded libraries compatible with Illumina systems were generated. The libraries were quantified using the Qubit dsDNA HS reagent kit and the Qubit 3.0 Fluorometer. Additionally, the average fragment sizes of the libraries were assessed using the Agilent High Sensitivity DNA Kit on the Agilent 2100 Bioanalyzer System (Agilent Technologies, Santa Clara, California). Subsequently, samples were sequenced on an Illumina MiSeq device with MiSeq Reagent Kit v3 (150-cycle) (Illumina, San Diego, California). CNV profiles were generated using an automated in-house pipeline which contains in brief the following steps: Trimming of raw FASTQ files with BBDuk 38.84 (JGI DataScience, BBtools software suite 2019 <https://jgi.doe.gov/data-and-tools/bbtools>), read decontamination using BioBloom Tools 2.0.13<sup>18</sup> mapping with Burrows-Wheeler Aligner (BWA-MEM algorithm 0.7.17) CNV profile



generation applying QDNAseq 1.26.0. After each step a quality control was performed (Table S1).<sup>19</sup>

## 2.11 | Panel sequencing

Eight micrometer-thick sections of FFPE primary tumor samples were analyzed by the Institute of Pathology (Technical University Munich, Germany) using a three primer pools yielding 617 amplicons covering mutational hotspot regions located in 353 exons of 59 genes that are known to be related to breast cancer as previously described.<sup>20</sup> Most relevant steps of the procedure are given in the Supporting Information Material. Quality assessment of panel sequencing is given in Table S2.

## 2.12 | GeparTrio patients' cohort for *mdm2* assessment

The GeparTrio trial (NCT00544765) was a multicenter, prospective, randomized, phase III trial with the primary goal to evaluate the pathologic complete response (pCR) after the treatment with four to six additional cycles of docetaxel, doxorubicin and cyclophosphamide (TAC) in patients responding to initially applied two cycles of TAC or four additional cycles of TAC compared to four cycles of vinorelbine and capecitabine for nonresponders to the initial two cycles of TAC. Patients with untreated primary breast carcinoma (T2-4, N0-3 and M0) were included.<sup>21</sup> pCR was defined as the absence of residual invasive and noninvasive disease in any excised breast or regional node tissue. For the analysis performed by our study we selected exclusively tissue specimens previously diagnosed as Luminal, that is, ER-positive BC. The categorization of Luminal-A and Luminal-B was based on a 20% Ki67 cut-off.<sup>22,23</sup> Overall, 502 Luminal BC specimens were subjected to our study. Two hundred and forty-five (48.8%) were attributed to the Luminal-A and 257 (51.2%) to Luminal-B sub-cohort. Relevant clinico-pathological characteristics of the patients' cohort are listed in Table S3. In addition, an assignment to samples with and without an *mdm2* gain is given.

## 2.13 | Selection of tissue samples, preparation of tissue microarrays and FISH

FISH on tumor tissue samples of the GeparTrio cohort was applied to tissue microarrays generated by the Institute of Pathology (Philipps-University Marburg). A ZytoLight SPEC MDM2/CEN12 dual color probe (ZytoVision GmbH, Bremerhaven, Germany) was used as previously described and samples from excised from HTM were done analogously.<sup>24</sup> More details are given in the Supporting Information Material. FISH results were categorized into the following Scoring system: Score 1:  $\approx 2$  *mdm2* gene signals, Score 2:  $\approx 5$  *mdm2* hybridization signals and Score 3: *mdm2* gain of  $\geq 10$ . The CEN12 marker

signals were disregarded since CEN12 alterations (either gains or losses) were not observed.

## 2.14 | Statistical analysis

DFS and OS were defined as the time (in months) from random assignment to the event; patients without event were censored at the time of the last contact.<sup>9,25</sup> Events for DFS were any locoregional (ipsilateral breast or local/regional lymph nodes) recurrence of disease, any contralateral breast cancer, any distant recurrence of disease, any secondary malignancy or death as a result of any cause, whichever occurred first. Event for OS was death due to any cause. Statistical tests applied are described in detail in the Supporting Information Material.

## 3 | RESULTS

### 3.1 | *mdm2* (or *mdm4*) gene amplification or a loss of TP53 is associated with engraftment in Luminal-B specific PDX

A total of seven Luminal-B specific humanized PDX were generated based on defined ER, progesterone receptor (PR) and HER2 expression patterns as given in Figure 1A. Accordingly, all PDX samples were ER-positive, four were ER/PR-double-positive and two samples were ER/HER2-double positive. Twenty-two tumor samples of Luminal-B patients derived from the Department of Gynecology at the University of Regensburg were transplanted in NSG mice from which two tumors led to a stable and retransplantable PDX model (PT-S1 and PT-E1). Overall, we achieved an engraftment rate of approximately 10%. Three previously established PDX models (PT-S2 [alias HBCx3], PT-S3 [alias HBCx22] and PT-S4 [alias HBCx34]; Institute Curie, Paris, France<sup>12</sup>) and two other models established at the German Cancer Research Center Heidelberg (PT-CTC and PT-E2<sup>2</sup>) were transferred into humanized mice and further evaluated.

Analysis of genomic alterations in these PDX models by panel sequencing revealed that all successfully engrafted tumors share genomic alterations within the *mdm2/mdm4/TP53* axis. More specifically, samples with the capacity for engraftment, harbored either an *mdm2* or *mdm4* gene amplification and/or a loss or mutation of TP53 as given in Figure 1A. Two models showed an additional HER2 gene amplification. *mdm2* FISH confirmed *mdm2* gene amplifications as initially determined by panel sequencing and revealed either  $\approx 5$  gene copies (ie, Score 2) or  $\geq 10$  copies (ie, Score 3) as defined in Section 2. Notably, as analyzed by FISH 95.0% (1/20) of not-engrafted tumor samples had no *mdm2* gene amplification (ie, Score 1, data not shown). Hereinafter, *mdm2* amplified PDX models are referred to as *mdm2*<sup>Amp</sup> and “*mdm2* wildtype” models are referred to as *mdm2*<sup>WT</sup>. Since the PT-E1 model was unique due to an inherent *mdm4* alteration we excluded this model from further analysis.

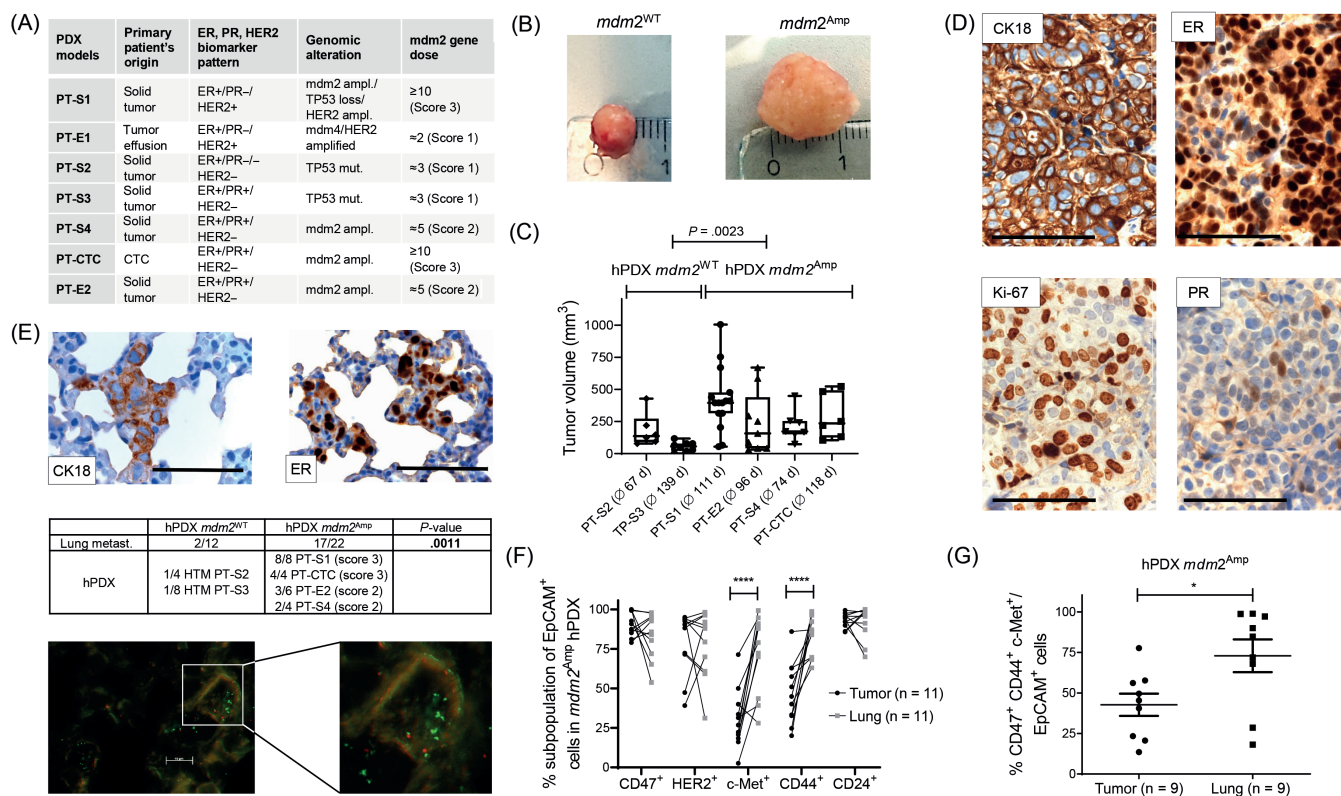


**FIGURE 1** Origin of seven Luminal-B humanized PDX models used in our study and tumor growth and lung metastases of *mdm2*<sup>WT</sup> and *mdm2*<sup>Amp</sup> transplanted hPDX. (A) Nomenclature of seven Luminal-B hPDX models use in our study is listed. In addition, genomic alterations of HER2, *mdm2*, *mdm4* and TP53 found upon successfully engrafted PDX tumor samples and the respective *mdm2* scores are given. CTC, generated from circulating tumor cells from the peripheral blood; E, generated from metastatic tumor effusion; PT, primary tumor material; S, generated from solid tumor. (B) Representative tumor samples from *mdm2*<sup>WT</sup> and *mdm2*<sup>Amp</sup> are displayed. (C) Tumor volume of *mdm2*<sup>WT</sup> and *mdm2*<sup>Amp</sup> in hPDX was assessed ( $\pi/6 \times \text{length} \times \text{width} \times \text{height}$ ) and significances between both groups were calculated by Student's t-test ( $P = .0023$ ). The average days of survival post tumor transplantation of each model are indicated in brackets. (D) Exemplary tumor samples stained for CK18, estrogen receptor (ER), Ki-67 and progesterone receptor (PR) are shown for PDX PT-S3. (E) Representative images of CK18 and ER expression on lung metastases in *mdm2*<sup>Amp</sup> transplanted PDX PT-S1 are displayed (upper panel). Bars represent 100  $\mu\text{m}$ . Lung tissues from individual hPDX models were stained with CK18 specific antibodies and the number of mice with detectable tumor cells was counted. The difference in incidence for lung metastases was calculated using the two-sided Fisher's exact test ( $P = .0011$ ). An example FISH image of lung metastatic cells (PDX model PT-S1) with *mdm2* gene amplification is shown. (F) Single cells from the lung and the corresponding tumor of *mdm2*<sup>Amp</sup> hPDX (PT-CTC, PT-S1 and PT-S4) were phenotypically analyzed using flow cytometry. Differences were calculated using Sidak's multiple comparisons test ( $****P < .0001$ ). (G) CD47<sup>+</sup>, CD44<sup>+</sup> and c-Met<sup>+</sup> positive cell populations in tumor and lung tissues of *mdm2*<sup>Amp</sup> hPDX were compared and statistical differences calculated by Student's t-test ( $*P < .05$ )

### 3.2 | *mdm2* amplified PDX was associated with an increased tumor volume and enhanced lung metastases in hPDX

Tumor samples from each PDX model were transplanted into NSG in the presence of a human immune system resulting in hPDX. The tumor volume in all four hPDX-*mdm2*<sup>Amp</sup> mouse models were significantly increased in comparison to hPDX-*mdm2*<sup>WT</sup> (Figure 1B,C;  $P = .0023$ ). A correlation between the origin of tumor models and tumor volume could be precluded. Immunohistochemical staining of cytokeratin 18 (CK18), ER and PR confirmed the origin of the implanted human tumor and Ki-67 expression represents the proliferative capacity of the tumor tissue (Figure 1D).

CK18 is highly expressed in epithelial cells of Luminal-B breast cancer. It served as a marker to identify tumor cells in distant organs

(ie, metastases in the lung, Figure 1E). In addition, the number of animals with lung metastasis was determined based on CK18 staining. Besides an increased tumor growth in *mdm2*<sup>Amp</sup>, *mdm2* amplification correlated with a significantly enhanced potential to develop lung metastasis.

Lung metastases were detected in 2 of 12 hPDX-*mdm2*<sup>WT</sup> mice and in 17/22 hPDX-*mdm2*<sup>Amp</sup> mice (Figure 1E;  $P = .0011$ ). Enhanced lung metastasis is seen in all *mdm2*<sup>Amp</sup> mice and does not depend on individual mouse models or the origin of individual tumors used for the generation of hPDX mice.

Notably, highly *mdm2* amplification (Score 3) seems to be associated with increased metastases within the *mdm2*<sup>Amp</sup> group (Score 3 = 100% metastases; Score 2 = 50% metastases formation; Figure 1E). *mdm2* gene amplification was also detectable in lung metastases (an example identified by FISH is given in the lower part of Figure 1E).

Single cells isolated from the tumor and the lung of hPDX *mdm2<sup>Amp</sup>* were phenotyped by flow cytometry and revealed a significant induction of c-Met and CD44 expression in metastatic tumor cells in the lung compared to primary tumor cells ( $P < .0001$ ; Figure 1F). CD44, CD47 and c-Met were found simultaneously upregulated in lung metastases of *mdm2<sup>Amp</sup>* PDX mice ( $P = .0252$ ; Figure 1G).

### 3.3 | *mdm2* gene amplification did not correlate with the frequency of tumor cell dissemination into the BM of hPDX

Single DTCs in the BM of mice were detected and quantified based on a panCK (CK8, CK18 and CK19) staining (Figure S1A). There was no significant difference in animals with detectable DTCs in the BM for *mdm2<sup>Amp</sup>* and *mdm2<sup>WT</sup>* models ( $P = .2929$ ; Figure S1A) and cells appeared as single cells or small clusters in both groups. The average frequency of detectable DTCs in 500,000 BM cells was 3.3 ( $\pm 0.97$  SEM;  $n = 7$ ). Just like metastatic tumor cells in the lung, DTCs in the BM showed a significantly increased CD44 and c-Met expression, which is exemplarily shown for *mdm2<sup>Amp</sup>* hPDX “PT-CTC” in Figure S1B (c-Met:  $P < .0001$ ; CD44:  $P < .0001$ ).

DTCs from three different hPDX BM samples and associated single cells from the corresponding tumors were isolated and subjected to low-pass genome sequencing. In contrast to isolated single resident BM cells, all isolated tumor cells from primary tumor and DTCs

showed copy number aberrations including an *mdm2* amplification (20/20; Figure S1C). However, the *mdm2* gene copy number varied in individual DTCs: One hPDX showed *mdm2* amplification also in the corresponding DTCs, one mouse showed gene amplification in two out of three DTCs and in one mouse all seven isolated DTCs lacked amplification (Figure S1C). While CK-negative single cells show a balanced profile (Figure S1D, upper profile), genomes of all isolated CK-positive cells have multiple genomic gains (depicted in red) and losses (depicted in blue). Interestingly, not only the *mdm2* gene region (chromosome 12) showed heterogeneity but also other loci indicated individual variation in between single cells isolated from the tumor and the different DTCs from the BM (Figure S1D).

### 3.4 | *mdm2* gene amplification reduced T cell incidence and maturation in hPDX

Analysis and phenotyping of immune cells was done for the two *mdm2<sup>WT</sup>* and four *mdm2<sup>Amp</sup>* models individually (Figure 2). Overall, Immune cell distribution in *mdm2<sup>Amp</sup>* hPDX revealed a significant reduced T cell fraction ( $P < .0001$ ) and increased B cell population ( $P < .0001$ ) in the spleen (Figure 2A) while variations between individual hPDX models are visualized. The T cell maturation of CD4<sup>+</sup> and CD8<sup>+</sup> was not significantly different within the *mdm2<sup>WT</sup>* and the *mdm2<sup>Amp</sup>* group as exemplarily shown for CD4<sup>+</sup> T cells (Figure 2B). Interestingly, *mdm2<sup>Amp</sup>* hPDX showed a significantly lower percentage of PD-1 expression on the CD8<sup>+</sup> T cells (Figure 2C, right graph;

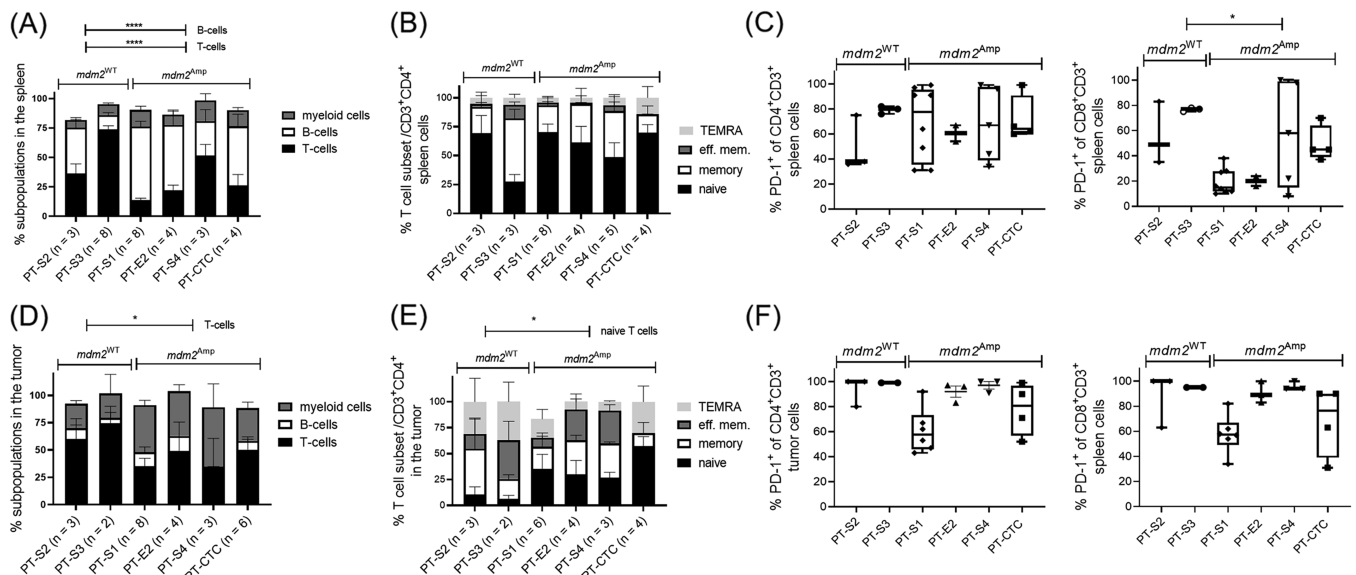


**FIGURE 2** Human immune cell reconstitution in *mdm2<sup>WT</sup>* and *mdm2<sup>Amp</sup>* transplanted hPDX. (A,B) Human immune cell distribution of myeloid, B and T cells, and T cell subsets (naïve, memory, memory effector and terminally differentiated effector memory cells [TEMRA]) in the spleen of individual *mdm2<sup>WT</sup>* and *mdm2<sup>Amp</sup>* hPDX models were determined using flow cytometry. (C) Graphs represent the percentage of PD-1 expression on CD4<sup>+</sup> (left graph) and on CD8<sup>+</sup> (right graph) T cells in the spleen. The immune subsets (D), T cell subpopulations (E) and PD-1 expression on CD4<sup>+</sup> and CD8<sup>+</sup> T cells (F) were analyzed in the tumor. Data are shown as mean  $\pm$  SEM and significances were analyzed using Sidak's multiple comparisons test (A, B, D, E) or Student's t-test (C, F).  $P$ -values  $< .05$  are indicated in the graphs (\* $P < .05$ ; \*\*\*\* $P < .0001$ ) and numbers of animals in each group are displayed ( $n = x$ ) or presented as individual symbol in the graphs

$P = .022$ ) but not on CD4<sup>+</sup> T cells (Figure 2C, left graph). The overall immune cell infiltration in the tumor tissue of ER-positive based hPDX was low (<1% CD45<sup>+</sup> cells; data not shown) and was nearly in the same low range as the fraction found in the primary tumor tissues of the tumor patients ( $\bar{0}$  7.83% CD45<sup>+</sup> cells  $\pm$  1.3 SEM;  $n = 11$ ; data not shown). The proportion of human T cells invading into the tumor tissue was also lower in *mdm2*<sup>Amp</sup> hPDX compared to *mdm2*<sup>WT</sup> hPDX (Figure 2D;  $P = .046$ ) while the percentage of naive CD4<sup>+</sup> T cells was significantly higher (Figure 2E;  $P = .045$ ). No differences could be detected with respect to CD8<sup>+</sup> T cells. Overall, a tendency of reduced PD-1 expression on CD4<sup>+</sup> and CD8<sup>+</sup> T cells in *mdm2*<sup>Amp</sup> hPDX in the tumor was seen, especially in the highly amplified (Score 3) hPDX models PT-S1 and PT-CTC (Figure 2F).

### 3.5 | *mdm2* knockdown and AMG232 based *mdm2* inhibition similarly induced apoptosis and reduced proliferation in ER-positive BC cells in vitro

The ER-positive cell line ZR-75-1 was treated with anti *mdm2* siRNA, which caused a significant depletion of the *mdm2* protein (Figure 3A). In addition, the FAK activity was diminished upon *mdm2* k.d. as indicated by a reduced phosphorylation, while the total FAK expression was not affected (Figure 3B). As a consequence of the primary siRNA based *mdm2* k.d. and the *mdm2* targeting with 1  $\mu$ M AMG232 significant fractions of apoptotic cells were observed (Figure 3C,  $P = .021$  and Figure 3D,  $P < .0001$ ). Moreover, the cell proliferation capacity was reduced upon *mdm2* k.d. (Figure 3E) as indicated by a reduced S-phase

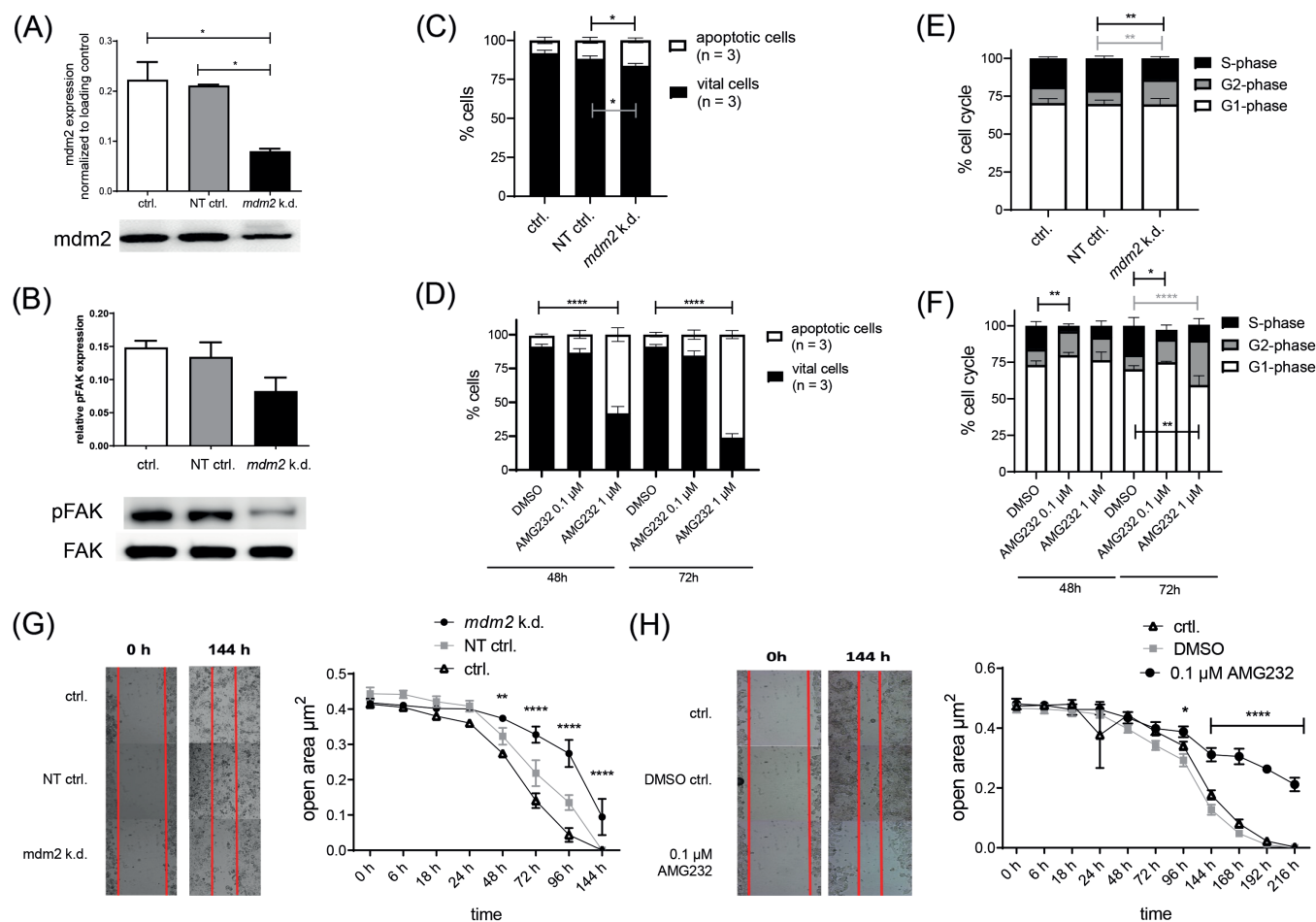


**FIGURE 3** Effects of *mdm2* knockdown and *mdm2* inhibition by AMG232 in breast cancer cells in vitro. The Luminal-B breast cancer cell line ZR-75-1 was treated with small-interfering RNA (siRNA) for *mdm2* (A, B, C, E, G) or with 0.1  $\mu$ M and 1  $\mu$ M AMG232 (D, F, H). (A,B) Western blotting of *mdm2* and FAK/pFAK expression of untreated (ctrl.), no target control RNA (NT ctrl.) or *mdm2* specific knockdown by siRNA (*mdm2* k. d.). Significant differences were calculated by Tukey's multiple comparisons test. Apoptosis induction upon *mdm2* k.d. (C) and AMG232 treatment (D) was analyzed by flow cytometry using an Annexin and DAPI staining to allow the differentiation of vital (Annexin<sup>-</sup> DAPI<sup>-</sup>) and dead cells (Annexin<sup>+</sup> and/or DAPI<sup>+</sup>). Data are shown as mean  $\pm$  SEM and Dunnett's multiple comparisons test was applied. Cell proliferation was analyzed upon *mdm2* k.d. (E) and AMG232 treatment (F) by flow cytometry and S-phase, G1 and G2 fraction were determined. Data are shown as mean  $\pm$  SEM and Dunnett's multiple comparisons test was applied. A scratch assay was performed upon *mdm2* siRNA (G) or AMG232 (H) treatment and ZR-75-1 with which cell migration capacity was analyzed over time. Data are shown as mean  $\pm$  SEM and Dunnett's multiple comparisons test was applied. Representative images show the time point after 144 hours of incubation. Red bars mark the gap after chamber removal at point 0 hour and the gap of *mdm2* k.d./AMG232 treatment after 144 hours. All experiments were performed three times and significances are indicated in each graph (\* $P < .05$ ; \*\* $P < .01$ ; \*\*\*\* $P < .0001$ ) [Color figure can be viewed at [wileyonlinelibrary.com](http://wileyonlinelibrary.com)]



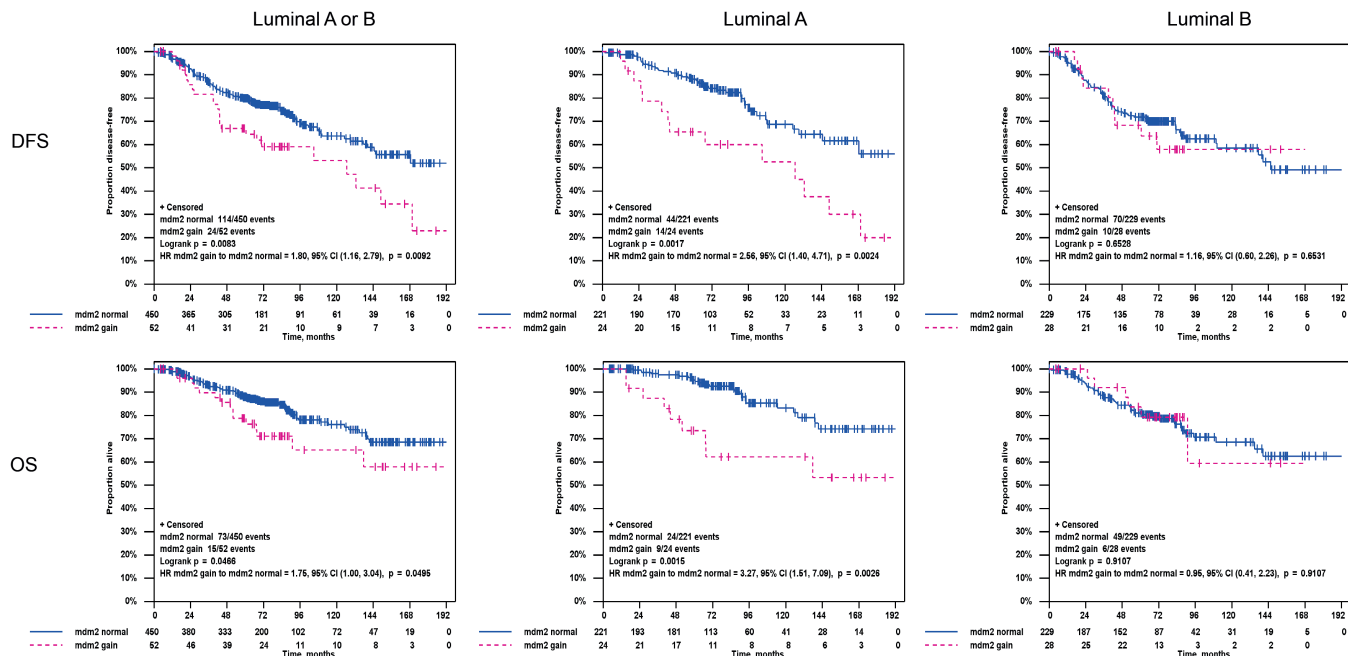


**FIGURE 4** DFS and OS in patients with *mdm2* gain vs no gain (ie, normal). Kaplan-Meier graphs illustrating course and outcome of Luminal BC disease as a function of *mdm2* gene amplification (Score 2 and 3) vs no amplification (Score 1) without and upon separation of Luminal-A vs Luminal-B BC as annotated. Both, DFS and OS was poor in association with an *mdm2* gain in the total cohort (DFS  $P = .008$ , OS  $P = .047$ ). Upon differentiation of Luminal-A vs Luminal-B cases statistical significance remained present for the Luminal-A cohort (DFS  $P = .002$ , OS  $P = .002$ ) but not for Luminal-B cohort (DFS  $P = .653$ , OS  $P = .911$ )

fraction ( $P = .0098$ ) accompanied by an elevated fraction of cells in the G2-phase of the cell cycle ( $P = .0074$ ). Similar results were obtained by the AMG232 treatment (Figure 3F), which also caused a reduced S-phase fraction (48 hours:  $P = .008$ , 72 hours:  $P = .049$ ) accompanied by a reduced G1-phase after 72 hours ( $P = .0027$ ) and an elevated fraction of G2 (Figure 3F,  $P < .0001$ ). Finally, cells with an *mdm2* k.d. and those exposed to *mdm2* targeting with AMG232 showed a delayed and retarded scratch overgrowth in the wound-healing assay (Figure 3G,H), which is compatible with the reduced FAK activity.

### 3.6 | DFS and OS of patients suffering from Luminal BC with an *mdm2* gain is poor compared to those without a gain

Microscopic images of *mdm2*/*cen12* FISH specimens scored 1, 2 or 3 are exemplarily shown in Figure S2. Patients with *mdm2* gain showed a significantly poor DFS (Figure 4; HR = 1.80 [95% confidence interval (CI): 1.16-2.79], log rank  $P = .008$ ) and OS (HR = 1.75 [95% CI: 1.00-3.05, log-rank  $P = .047$ ) compared to the patients without *mdm2* gain in the entire Luminal BC cohort. Similar results were observed in patients with Luminal-A BC (DFS: HR = 2.56 [95% CI: 1.40-4.71],  $P = .002$ ; OS: HR = 3.27 [95% CI: 1.51-7.09], log-rank  $P = .002$ ) but not within the Luminal-B subcohort (DFS: HR = 1.16 [95% CI: 0.60-2.26], log-rank  $P = .653$ ; OS: HR = 0.95 [95% CI: 0.41-2.23], log-rank  $P = .911$ ). Thus, an unfavorable impact of an *mdm2* gain on survival outcome within the entire Luminal BC cohort is mainly caused within the Luminal-A BC cohort.

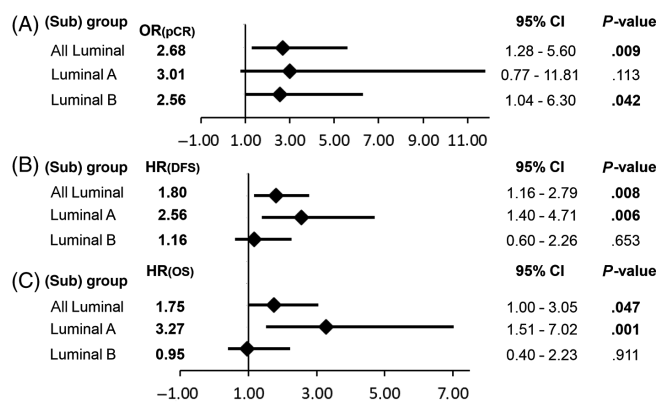


**FIGURE 5** Odds ratio of pCR and HRs of DFS and OS of Luminal BC patients as a function of *mdm2* status. Impact of an *mdm2* gain on (A) the pCR, (B) the DFS and (C) the OS of Luminal BC disease with and without differentiation of Luminal-A vs Luminal-B.  $P$ -value less than .05 indicate a significant impact of an *mdm2* gain on these parameters and are typed bold. DFS, disease-free survival; HR, hazard-ratio; OR, odds-ratio; OS, overall survival; pCR, pathological complete response

### 3.7 | Patients suffering from Luminal BC with *mdm2* gain (Score 2 or 3) show a higher complete pathological response rate but a worse DFS and OS

Overall, 53 (10.5%) of all Luminal BC patients included in our study experienced a complete pathological response (pCR) rate upon neoadjuvant treatment (Table S4). With respect to *mdm2*, the pCR rate of

TABLE 1 Multivariate analysis for pCR, DFS and OS

Multivariate analysis for pCR ↓				
Analysis set/parameter	Category	Odds ratio (OR)	95% CI	P-value
All Luminal				
<i>mdm2</i>	<i>mdm2</i> gain vs normal	3.01	1.36-6.64	.007
Age, years	>50 vs ≤50	0.79	0.42-1.51	.480
cT	cT3-4 vs cT1-2	0.87	0.42-1.81	.705
cN	cN+ vs cN–	0.90	0.47-1.70	.739
Grading	G3 vs G1-2	2.02	1.05-3.86	.034
Histotype	Nonductal vs ductal invasive	0.56	0.13-2.43	.437
Luminal-A				
<i>mdm2</i>	<i>mdm2</i> gain vs normal	2.02	0.39-10.47	.401
Age, years	>50 vs ≤50	0.75	0.23-2.44	.629
cT	cT3-4 vs cT1-2	1.03	0.26-4.14	.963
cN	cN+ vs cN–	0.94	0.28-3.20	.926
Grading	G3 vs G1-2	0.82	0.17-3.93	.800
Histotype	Nonductal vs ductal invasive	0.86	0.10-7.15	.891
Luminal-B				
<i>mdm2</i>	<i>mdm2</i> gain vs normal	3.75	1.42-9.87	.008
Age, years	>50 vs ≤50	0.80	0.36-1.76	.572
cT	cT3-4 vs cT1-2	0.73	0.30-1.74	.474
cN	cN+ vs cN–	0.72	0.33-1.57	.409
Grading	G3 vs G1-2	2.25	1.02-4.97	.044
Histotype	Nonductal vs ductal invasive	0.45	0.06-3.60	.451
Multivariate analysis for DFS ↓				
Analysis set/parameter	Category	HR	95% CI	P-value
All Luminal				
<i>mdm2</i>	<i>mdm2</i> gain vs normal	1.71	1.08-2.71	.022
Age, years	>50 vs ≤50	1.38	0.98-1.94	.068
cT	cT3-4 vs cT1-2	1.91	1.33-2.74	.000
cN	cN+ vs cN–	1.51	1.06-2.15	.022
Grading	G3 vs G1-2	0.86	0.58-1.28	.453
Histotype	Nonductal vs ductal invasive	1.38	0.78-2.47	.271
Luminal-A				
<i>mdm2</i>	<i>mdm2</i> gain vs normal	2.94	1.55-5.59	.001
Age, years	>50 vs ≤50	0.78	0.46-1.34	.370
cT	cT3-4 vs cT1-2	1.82	1.00-3.31	.049
cN	cN+ vs cN–	1.10	0.63-1.92	.746
Grading	G3 vs G1-2	0.98	0.50-1.91	.943
Histotype	Nonductal vs ductal invasive	1.48	0.62-3.52	.380
Luminal-B				
<i>mdm2</i>	<i>mdm2</i> gain vs normal	0.99	0.49-2.00	.985
Age, years	>50 vs ≤50	2.38	1.50-3.78	.000
cT	cT3-4 vs cT1-2	1.90	1.19-3.04	.007
cN	cN+ vs cN–	1.64	1.01-2.68	.046
Grading	G3 vs G1-2	0.71	0.43-1.17	.174
Histotype	Nonductal vs ductal invasive	1.37	0.62-3.01	.437
Multivariate analysis for OS ↓				
Analysis set/parameter	Category	HR	95% CI	P-value
All Luminal				
<i>mdm2</i>	<i>mdm2</i> gain vs normal	1.39	0.77-2.50	.272



TABLE 1 (Continued)

Multivariate analysis for OS ↓					
Analysis set/parameter	Category	HR	95% CI	P-value	
Age, years	>50 vs ≤50	1.94	1.25-3.01	.003	
cT	cT3-4 vs cT1-2	2.04	1.30-3.18	.002	
cN	cN+ vs cN-	1.93	1.22-3.04	.005	
Grading	G3 vs G1-2	1.02	0.64-1.64	.935	
Histotype	Nonductal vs ductal invasive	1.05	0.48-2.29	.911	
Luminal-A					
mdm2	mdm2 gain vs normal	3.20	1.35-7.59	.008	
Age, years	>50 vs ≤50	1.29	0.64-2.60	.485	
cT	cT3-4 vs cT1-2	1.94	0.88-4.31	.102	
cN	cN+ vs cN-	1.40	0.65-3.00	.388	
Grading	G3 vs G1-2	1.00	0.43-2.33	.997	
Histotype	Nonductal vs ductal invasive	1.65	0.56-4.91	.365	
Luminal-B					
mdm2	mdm2 gain vs normal	0.67	0.27-1.70	.400	
Age, years	>50 vs ≤50	2.90	1.63-5.17	<.001	
cT	cT3-4 vs cT1-2	1.88	1.07-3.29	.028	
cN	cN+ vs cN-	2.02	1.10-3.71	.023	
Grading	G3 vs G1-2	0.81	0.45-1.46	.487	
Histotype	Nonductal vs ductal invasive	0.75	0.23-2.44	.634	

Luminal BC patients with *mdm2* gain (Score 2 or 3) was 21.2% vs 9.2% within the group of patients without enhanced *mdm2* (OR = 2.68 [95% CI: 1.28-5.60], *P* = .009; Figure 5A). Similarly, the pCR rate was significantly higher in the presence of an *mdm2* gain for the Luminal-B subcohort (Figure 5A; 28.6% vs 13.4%, OR = 2.56 [95% CI: 1.04-6.30], *P* = .042) compared to those with an unaltered *mdm2* status. This finding was not significant for Luminal-A BC patients: (Figure 5A; 12.5% vs 4.6%, OR = 3.01 [95% CI: 0.77-11.81], *P* = .113). The HR for DFS (Figure 5B) in the presence of *mdm2* gain was also higher for all Luminal (HR [DFS] = 1.80 [95% CI: 1.16-2.79], *P* = .008) and for Luminal-A patients (HR [DFS] = 2.56 [95% CI: 1.40-4.71], *P* = .006). The HR (OS) for all Luminal patients was 1.75 ([95% CI: 1.00-3.05], *P* = .047) and remained significant for Luminal-A patients only (Figure 5C; HR [OS] = 3.27 [95% CI: 1.51-7.02], *P* = .001).

In the multivariate analysis for pCR (Table 1), an *mdm2* amplification remained a significant predictor of pCR in all Luminal BC samples (ie, cumulated Luminal-A and Luminal-B; OR = 3.01 [95% CI: 1.36-6.64], *P* = .007) and within the Luminal-B subcohort (OR = 3.75 [95% CI: 1.42-9.87], *P* = .008). With regards to survival outcomes the multivariate analysis revealed that an *mdm2* gain added a significant prognostic value to the DFS (Table 1) in all Luminal BC (HR = 1.71 [95% CI: 1.08-2.71], *P* = .022) and in the Luminal-A only cohort (HR = 2.94 [95% CI: 1.55-5.59], *P* = .001). In the multivariate analysis for OS (Table 1) a significant negative prognostic value of elevated *mdm2* remained in the Luminal-A subcohort (HR = 3.20 [95% CI: 1.35-7.59], *P* = .008). An impact of patients' age was seen with respect of DFS in the Luminal-B cohort (HR = 2.38 [95% CI: 1.50-3.78], *P* = .000). Patients age had a significant impact on the OS

of the total Luminal cohort (HR = 1.94 [95% CI: 1.25-3.01], *P* = .003) and upon separate analysis in the Luminal-B cohort only (HR = 2.90 [95% CI: 1.63-5.71], *P* < .001).

### 3.8 | A moderate *mdm2* gain (≈5 gene copy numbers) had an unfavorable effect on Luminal-A BC patients while an enhanced *mdm2* gain (≥10 gene copy numbers) unfavorably affects the long-term outcome predominantly of Luminal-B BC disease

The impact of a pronounced *mdm2* gene dose (ie, Score 3) on the survival outcome of Luminal BC disease has been separately evaluated (Figure S3). Kaplan-Meier curves demonstrate that a pronounced gain unfavorably affected both the DFS (HR = 2.83 [95% CI: 1.38-5.80], log-rank *P* = .003) and the OS (HR = 2.66 [95% CI: 1.08-6.58], log-rank *P* = .028) of all Luminal BC patients, however, among Luminal-A and Luminal-B cohorts this effect remained only significant for the DFS in Luminal-B patients (HR = 3.16 [95% CI: 1.27-7.88], log-rank *P* = .009).

The overall differentiation of Luminal-A and Luminal-B BC samples without (Score 1), with a moderate (Score 2) and with an enhanced *mdm2* gain (Score 3) revealed a significant unfavorable impact of a moderate *mdm2* gain both on the DFS (HR = 2.55 [95% CI: 1.30-5.00], log-rank *P* = .004) and OS (HR = 3.22 [95% CI: 1.38-7.55], log-rank *P* = .005) but only in Luminal-A patients (Figure S4). In contrast, a pronounced *mdm2* gain takes effect only on the DFS (HR = 3.08 [95% CI: 1.23-7.70], log-rank *P* = .01) in

Luminal-B BC patients. Of note, these results should be interpreted with caution due to the small number of events.

### 3.9 | The survival outcome of Luminal-B BC disease was poor compared to the Luminal-A BC disease regardless the *mdm2* status

Without taking the *mdm2* status into account Kaplan-Meier showed that both the DFS (HR Luminal-B to Luminal-A = 1.63 [95% CI: 1.16-2.29], log-rank  $P = .004$ ) and OS (HR Luminal-B to Luminal-A = 1.95 [95% CI: 1.26-3.00], log-rank  $P = .002$ ) were poor in Luminal-B BC patients compared to Luminal-A BC (Figure S5).

## 4 | DISCUSSION

The differentiation of ER-positive BC cancers to either the Luminal-A or Luminal-B subtype is useful but insufficient for judging the patients' individual risk to experience tumor progression and relapse. Thus, Luminal BC requires further stratification that allows improved individual prognosis and therapy. Here we analyzed tumor engraftment, growth and progression in a human-like preclinical mouse model to identify biomarkers associated with high-risk Luminal BC disease. Essentially, we identified that an increased *mdm2* gene copy number was associated with successful tumor engraftment in humanized NSG mice while nonengrafted tumors had basically an unaltered *mdm2*. Moreover, these mice had an increased rate and size of lung metastasis which was characterized by a pronounced c-Met, and CD44 expression.

A CD44<sup>high</sup>/CD24<sup>low</sup> phenotype has been repeatedly attributed to BC stem cells with pronounced resistance to various treatments and enhanced tumorigenicity.<sup>26</sup> However, it is becoming more and more obvious that this phenotype alone may not appropriately envisage the initiation of tumor growth, progression and metastasis.<sup>27-30</sup> Moreover, a number of functional studies unambiguously indicate that an elevated CD44/CD24 expression ratio taken alone is neither sufficiently representative for the colony forming capacity in vitro nor for the initiating of tumor growth in vivo.<sup>15,31,29,32</sup> Thus, a multifactorial phenotype and genotype that includes a variety of markers known to be not only involved in but also to be essential for tumor stemness can be considered more robust to predict onset of tumor growth or tumor relapse after therapy. c-Met, CD44 and CD47 have been previously described to be part of an enhanced capacity to initiate metastasis of Luminal BC in a preclinical mouse model.<sup>15</sup> The analysis of a small cohort of metastatic Luminal BC patients revealed that in particular the presence of CD44/c-Met/CD47 triple positive CTCs correlate with dismal survival and increased metastasis.<sup>2</sup> Engraftment rates of Luminal tumors in mice (PDX) are generally low.<sup>33</sup> Success rates less than 5% have been reported.<sup>11</sup> Interestingly, in our study only tumor samples from patients with an altered *mdm2*, *mdm4* or TP53 genotype had the capacity to engraft in humanized mice pointing to the more aggressive characteristic of these tumors. Moreover, using humanized

NSG based xenotransplants we found here that mice transplanted with *mdm2* amplified tumors not only showed increased tumor growth than animals transplanted with tumors without *mdm2* alteration, but also they had a significantly higher rate of (lung) metastasis (77.3% vs 16.7%). In addition, CD44 and c-Met were significantly higher expressed in metastatic cells compared to the primary hPDX tumor. Thus, we conclude that in addition to a pronounced CD44 and c-Met expression an *mdm2* gene amplification determines an enhanced malignant capacity of Luminal BC cells in a preclinical human-like in vivo setting.

Comparative low pass sequencing of DTCs and selected tumor cells revealed *mdm2*<sup>Amp</sup> primary tumors harbored *mdm2* amplifications in all analyzed single cells while a number of corresponding single DTCs isolated from BM displayed an *mdm2*<sup>WT</sup> genotype. Regarding the complex genomic rearrangements on chromosome 12, it is unlikely that DTCs have lost the *mdm2* amplification after their dissemination. Instead, the tumor might also harbor a low frequency of subclones without *mdm2* amplification. Especially the observation in model hPDX PT-S1, which showed exclusively *mdm2*<sup>WT</sup> DTCs in BM could indicate a parallel progression of tumor cells with different genotype.<sup>34</sup> This suggests that hPDX models could mimic human disease in which primary tumors and DTCs have been shown to be highly heterogeneous.<sup>35</sup>

HTM, based on cell lines or patient derived tumor xenografts allow the evaluation of immune cell status as a function of treatment. In our study, human T cell incidence, PD-1 expression, tumor infiltration, maturation and activation were diminished in *mdm2*<sup>Amp</sup> hPDX, which additionally indicates an *mdm2*-dependent immune cell regulation. Recent studies demonstrated a potential immune inhibitory effect of *mdm2*. It has been reported, for example, that co-targeting of the aurora kinase-A and *mdm2* results in inhibited tumor growth in a murine melanoma model and four melanoma PDX models, which was associated with an enhanced infiltration of NK and antigen presenting cells into the murine tumors.<sup>36</sup> Thus, targeting *mdm2* (eg, with molecule specific inhibitors) in combination with other treatments might be a promising strategy to treat Luminal BC with an *mdm2* gain. Moreover, Fang et al detected the synergistic effect of inhibiting *mdm2* with APG115 in combination with a PD-1 blockade, which resulted in enhanced immune cell activation and infiltration of cytotoxic T cells. In addition, they observed polarization of M1 macrophages by inhibition of M2 differentiation.<sup>37</sup> Alternatively, Zou et al stabilized *mdm2* by the deubiquitinases USP15, which reduced T cell activation.<sup>38</sup>

Mechanistically, the interaction of *mdm2* and TP53 seems to be essential too. *mdm2* is known as an antagonist to regulate both the protein content and activity of the tumor suppressor TP53.<sup>39</sup> As an E3 ubiquitin ligase *mdm2* induces TP53 degradation but also suppresses the TP53 transactivation domain and thereby attenuates the transcriptional activity of TP53. A reduced TP53 expression and activity results in a loss of cell cycle control and a reduced ability of proliferating cells to initiate the repair of DNA damages or cell death.<sup>40</sup> Thus, the "guardian role" of TP53 becomes impaired by an excessive presence and activity of *mdm2*. With view to these molecular

mechanisms it is not surprising that *mdm2* gene amplification and elevated *mdm2* expression levels have been formerly associated with tumorigenesis and an increased incidence of malignant diseases.<sup>41-43</sup> A negative prognostic impact in BC has been described as well.<sup>44</sup>

The transcription factor TP53 is not only an important player in the regulation of cell-cycle and apoptosis but also has been shown to manipulate the tumor-immune cell crosstalk. For example, TP53 has been described to modulate the differentiation of macrophages towards an antitumor M1 by preventing the immunosuppressive M2 phenotype.<sup>45</sup> Previously, Wang et al described the effect of a second generation *mdm2* inhibitor (HDM201) in a murine syngenic mouse model that resulted in an increased DC population, enhanced infiltration of T-bet<sup>+</sup>/Eomes<sup>+</sup> CD8<sup>+</sup> T cells and raised the CD8/T<sub>reg</sub> ratio. These effects were reversed using TP53 knockout tumor cells. Furthermore, the activation marker CD80 was elevated on tumor cells associated with enhanced IFN $\gamma$  release and T cell mediated tumor cell killing.<sup>46</sup> In addition, the generation of apoptotic cells by an inhibition of *mdm2* (as shown in our study) might cause the release of tumor antigens, which might further boost an immunological tumor defense. Different clinical trials using *mdm2* inhibitors such as AMG232 are ongoing (eg, acute myeloid leukemia NCT04190550; glioblastoma NCT03107780). Solid tumor entities as ER-positive metastatic BC with *mdm2* overexpression are also being addressed.<sup>47</sup> Moreover, the inhibition of *mdm2* and PD-1 (pembrolizumab) is being investigated in clinical trials (NCT03611868) and novel therapeutic combinations therapies for ER-positive BC patients are subject to preclinical studies (anti-CDK4/6 plus anti-*mdm2*).<sup>48</sup> Remarkably, *mdm2* does not only develop TP53-dependent activity but also can potentiate tumor growth and progression TP53-independently. More specifically, *mdm2* physically interacts with the ER and can enhance its' transcriptional (and thus the proproliferative) activity in an estradiol-dependent fashion.<sup>49</sup> Consequently, *mdm2*-mediated downregulation and deactivation of TP53 and the *mdm2*-mediated direct ER-transactivation have a mutually reinforcing effect that results in a growth advantage of Luminal BC. Thus, the TP53-dependent and independent activities affect growth and progression of Luminal BC.

Extending our preclinical in vivo studies on hPDX we cytogenetically detected an *mdm2* gain in 10.5% of Luminal BC patients within the GeparTrio trial.<sup>9</sup> The gain of the *mdm2* gene region detected by FISH can be interpreted as *mdm2* gene amplification since in respective tissue specimens the corresponding centromere 12 region was never found simultaneously increased. BCs (10.5%) with *mdm2* gene amplification is in agreement with various studies by which an incidence of enhanced *mdm2*—either on the genomic or the protein level—in the range of 5.7% to 15.0% has been reported.<sup>39,41,50,51</sup> Taken the whole Luminal BC cohort of our study without differentiating between Luminal-A and Luminal-B both the DFS and OS was poorer for those patients with *mdm2* amplified breast cancer. Upon separate evaluation of Luminal-A and Luminal-B fraction this finding remained significant and therefore valid for Luminal-A BC patients only. In contrast, a pronounced *mdm2* amplification (ie, only Score 3) has a negative impact on the DFS only of BC patients suffering from the Luminal-B subtype. This observation is based on a Score

3 frequency of 4.0% in Luminal-B BC, which is just slightly higher than in the Luminal-A cohort (2.4%). Accordingly, the missing significance of an enhanced *mdm2* gain (ie, Score 3) on the course of disease of Luminal-A BC patients might be due to the low number of those cases within this subcohort. However, it can be speculated that within the Luminal-B cohort only an enhanced (but not a moderate) gain has an extra impact on the course of disease, because this BC subtype inherently comes with a poorer prognosis compared to the Luminal-A patient group, an observation that has been repeatedly reported formerly.<sup>52</sup> The clinical appearance of Luminal-A BC has been frequently associated to a rather high ER-expression, while the Luminal-B type shows less ER-expression but an enhanced proliferation activity, typically represented by higher Ki67 values.<sup>3,6</sup> Accordingly, a favorable and unfavorable long-term outcome of the Luminal-A vs Luminal-B BC subgroups within the GeparTrio study, which was *mdm2* independent, has been confirmed in our study (Figure S5). However, we here generated evidence that also an *mdm2* dose-dependent effect takes place in Luminal-B BC. One can assume that the higher the *mdm2* protein expression is the more efficient is the deactivation of TP53, which might correlate with an enhanced tumor cell viability. This consideration is supported by previous studies that addressed the impact of the *mdm2* gene dose, the extent of *mdm2* protein expression and the cellular localization.<sup>44,53</sup>

The long-term outcome in our study was generally disadvantageous for patients suffering from tumors with an *mdm2* gene amplification although the pCR rates were significantly higher for these patients compared to the cohort without an *mdm2* gain (Figure 5). This finding is valid for the total Luminal BC cohort from the GeparTrio trial subjected to our study and upon Luminal-A/Luminal-B separation for Luminal-B BC patients. An enhanced primary effect of cytotoxic treatments in Luminal BC with *mdm2* amplification might again be explained by higher proliferation capacity of responsive tumors that is further enhanced by an elevated presence of *mdm2*. However, an initially better pCR that does finally not result in an improved outcome (OS) of disease, an observation that might be due to a very long observation time of the course of disease that was 200 months in our study (Figure 5). However, different therapy regimens were not considered in our study as the treatment adaptation due to an insufficient response that improved DFS and OS of patients with hormone receptor positive BC. Both aspects could potentially explain the individual neoadjuvant treatment response vs long-term outcome.<sup>9,54</sup> Nevertheless, a pronounced *mdm2* gene dose (ie, Score 3) is associated to a better initial treatment response but seems on long-term to be somehow involved in an unfavorable outcome. Even though Luminal BC is basically characterized by an advantageous prognosis suffering from this BC subtype it is considered as a long-term disease that tends to progress by relapse or metastasis rather later not sooner. An *mdm2* activity might contribute to such a late progress of disease.

In conclusion, an *mdm2* gene amplification facilitates growth and progression of estrogen receptor-positive BC growth in a preclinical xenograft humanized NSG mouse model. *mdm2* inhibition in vitro reduced malignant cell proliferation and migration and induced tumor cell apoptosis. In addition, an *mdm2* gain is strongly associated with an unfavorable outcome of Luminal BC disease. Prospective studies

are required to verify the suitability of *mdm2* for advanced Luminal BC stratification and therapeutic targeting.

## ACKNOWLEDGMENTS

We would also like to thank Gerhard Piendl, Stephan Seitz, Elisabeth Inwald, Theresa Plach and Maria Hutterer (all Department of Gynecology and Obstetrics, University of Regensburg) for their excellent support. We are also grateful to Massimo Saini (formerly German Cancer Research Center, Heidelberg, Germany) for his valuable advice. We would like to thank Christoph Klein (Experimental Medicine and Therapy Research, University of Regensburg, Division of Personalized Tumor Therapy, Fraunhofer Institute for Toxicology, Regensburg, Germany) and Wilko Weichert (Institute of Pathology, Technical University Munich, Germany) for supporting this project and for helpful advice. We appreciate the work of Lenny Shultz (The Jackson Laboratory, USA) for providing access to NSG mice. We also thank Matthias Evert for generating immunohistological specimens from paraffin embedded tissue sections (Institute of Pathology, University of Regensburg) and Marion Schweiger, (University of Regensburg) for her assistance in graphical design. Our study was funded by the Deutsche Krebshilfe (Deutsche Krebshilfe, “TransLUMINAL-B” project, funding no.: 111536).

## CONFLICT OF INTEREST

Gero Brockhoff and Anja Kathrin Wege: Patent pending outside this work: EP16168619.1. Paul Jank: Stock ownership from Myriad Genetics, Inc., outside the submitted work. Carsten Denkert: Personal fees from Novartis, personal fees from Roche, MSD Oncology, Daiichi Sankyo, AstraZeneca and Merck. Grants from Myriad Genetics, other from Sividon Diagnostics/Myriad, outside the submitted work; Patents pending: WO2020109570A1—cancer immunotherapy. Patents issued: WO2015114146A1 and WO2010076322A1—therapy response. Patents royalty: VMscope digital pathology software. Volker Möbus: Speaker honoraria received from Amgen, AstraZeneca, Celgene, Roche, Teva. Consultancy honoraria from Roche, Amgen, Tesaro, Myelo Therapeutics. Marion van Mackelenbergh: personal fees/honoraria from Amgen, AstraZeneca, Daiichi Sankyo, Genomic Health, Gilead, GSK, Lilly, Molecular Health, Mylan, Novartis, Pfizer, Pierre Fabre, Roche, Seagen. Jens-Uwe Blohmer: Presentations and/or advisory board: AstraZeneca, Amgen, ExactSciences, MolecularHealth, Lilly, MSD, Novartis, Pfizer, Roche, Seagen, Sysmex, SonoScape. Nicole Pfarr: Speaker Fee & Traveling Support: AstraZeneca, Illumina, Thermo Fisher Scientific, Roche, Bristol Myers Squibb; Advisory Board: Bayer, Lilly, Novartis, Roche. Sibylle Loibl: Honorarium for Advisory Board and grant paid to the institute from Abbvie, AstraZeneca, Celgene, Immunomedics/Gilead, Novartis, Pfizer, Roche. Honorarium for Advisory Board and others paid to the institute from Amgen, Bayer, BMS, Eisgenix, GSK, Lilly, Merck, Pierre Fabre, Prime/Medscape, Puma, Samsung, Seagen. Patents: EP14153692.0 (pending), EP21152186.9 (pending), EP15702464.7 (issued), EP19808352.8 (pending), Digital Ki67 Evaluator (VM Scope GmbH). Olaf Ortmann: Stock and other ownership interests from Novartis, Fresenius. Honorarium for Advisory Board from VFA, AstraZeneca, Novartis, Roche, Tesaro, Pfizer, Aurikamed. Other coauthors do not declare any potential conflicts of interest.

## AUTHOR CONTRIBUTIONS

Anja Kathrin Wege and Gero Brockhoff: Study design and supervision, principle investigators, data analysis, article writing. Eva-Maria Rom-Jurek: Mouse and in vitro experiments, data analysis. Paul Jank and Carsten Denkert: Data interpretation, article proof reading. Peter Ugocsai: Provided cord blood and tumor samples for the generation of hPDX. Christine Solbach, Jens-Uwe Blohmer, Bruno Sinn, Marion van Mackelenbergh and Volker Möbus provided tumor tissues as well as clinicopathological and follow-up data to the GeparTrio trial. Andreas Trumpp and Elisabetta Marangoni: Provided initial PDX models. Nicole Pfarr: Panel sequencing. Christoph Irlbeck and Bernhard Polzer: DTC analyses and data interpretation. Jens Warfsmann: Bioinformatic data analysis of low-pass sequencing. Florian Weber: Tumor and tissue preparation of hPDX transplantation and FISH experiments. Olaf Ortmann and Sibylle Loibl: Contributed to the article text. Valentina Vladimirova: Statistical analysis and article proof-reading.

## DATA AVAILABILITY STATEMENT

Data that support the findings of our study are available from the corresponding author upon request.

## ETHICS STATEMENT

Cord blood samples were obtained based on the approval given by the Ethics Committee of the University of Regensburg (permission number 17-527-101). All patients provided informed written consent. Patient derived tissues samples were used based on written consent by every patient and based on the permission of the Ethics Committee of the University of Regensburg (permission number: 14-101-0063). The local veterinary authorities of the district government of Lower Franconia and Upper Palatinate (Bavarian region) approved all animal experiments (permission no. 54-2532-1-16/14 and 55.2 DMS-2532-2-422).

## ORCID

Bernhard Polzer  <https://orcid.org/0000-0002-3797-9975>

Gero Brockhoff  <https://orcid.org/0000-0001-8398-8349>

## REFERENCES

- Wege AK, Ernst W, Eckl J, et al. Humanized tumor mice: a new model to study and manipulate the immune response in advanced cancer therapy. *Int J Cancer*. 2011;129(9):2194-2206.
- Baccelli I, Schneeweiss A, Riethdorf S, et al. Identification of a population of blood circulating tumor cells from breast cancer patients that initiates metastasis in a xenograft assay. *Nat Biotechnol*. 2013;31:539-544.
- Harbeck N, Penault-Llorca F, Cortes J, et al. Breast cancer. *Nat Rev Dis Primers*. 2019;5:66.
- Perou CM, Sørlie T, Eisen MB, et al. Molecular portraits of human breast tumours. *Nature*. 2000;406:747-752.
- Eroles P, Bosch A, Pérez-Fidalgo JA, Lluch A. Molecular biology in breast cancer: intrinsic subtypes and signaling pathways. *Cancer Treat Rev*. 2012;38:698-707.
- Villegas SL, Nekljudova V, Pfarr N, et al. Therapy response and prognosis of patients with early breast cancer with low positivity for

- hormone receptors: an analysis of 2765 patients from neoadjuvant clinical trials. *Eur J Cancer*. 2021;148:159-170.
7. Loibl S, Poortmans P, Morrow M, Denkert C, Curigliano G. Breast cancer. *Lancet*. 2021;397:1750-1769.
  8. Pan H, Gray R, Braybrooke J, et al. 20-year risks of breast-cancer recurrence after stopping endocrine therapy at 5 years. *N Engl J Med*. 2017;377:1836-1846.
  9. Minckwitz G von, Blohmer JU, Costa SD, et al. Response-guided neoadjuvant chemotherapy for breast cancer. *J Clin Oncol*. 2013;31:3623-3630.
  10. Al-Hajj M, Wicha MS, Benito-Hernandez A, Morrison SJ, Clarke MF. Prospective identification of tumorigenic breast cancer cells. *Proc Natl Acad Sci U S A*. 2003;100:3983-3988.
  11. Marangoni E, Vincent-Salomon A, Auger N, et al. A new model of patient tumor-derived breast cancer xenografts for preclinical assays. *Clin Cancer Res*. 2007;13:3989-3998.
  12. Cottu P, Marangoni E, Assayag F, et al. Modeling of response to endocrine therapy in a panel of human luminal breast cancer xenografts. *Breast Cancer Res Treat*. 2012;133:595-606.
  13. Reyaf F, Guyader C, Decraene C, et al. Molecular profiling of patient-derived breast cancer xenografts. *Breast Cancer Res*. 2012;14:R11.
  14. Cottu P, Bièche I, Assayag F, et al. Acquired resistance to endocrine treatments is associated with tumor-specific molecular changes in patient-derived luminal breast cancer xenografts. *Clin Cancer Res*. 2014;20:4314-4325.
  15. Baccelli I, Stenzinger A, Vogel V, et al. Co-expression of MET and CD47 is a novel prognosticator for survival of luminal breast cancer patients. *Oncotarget*. 2014;5:8147-8160.
  16. Wege AK, Dreyer TF, Teoman A, Ortmann O, Brockhoff G, Bronger H. CX3CL1 overexpression prevents the formation of lung metastases in Trastuzumab-treated MDA-MB-453-based humanized tumor mice (HTM). *Cancer*. 2021;13(18):2459-2478.
  17. Silvestri M, Reduzzi C, Feliciello G, et al. Detection of genomically aberrant cells within circulating tumor microemboli (CTMs) isolated from early-stage breast cancer patients. *Cancer*. 2021;13(6):1409-1428.
  18. Chu J, Sadeghi S, Raymond A, et al. BioBloom tools: fast, accurate and memory-efficient host species sequence screening using bloom filters. *Bioinformatics (Oxford, England)*. 2014;30:3402-3404.
  19. Scheinin I, Sie D, Bengtsson H, et al. DNA copy number analysis of fresh and formalin-fixed specimens by shallow whole-genome sequencing with identification and exclusion of problematic regions in the genome assembly. *Genome Res*. 2014;24:2022-2032.
  20. Pfarr N, Penzel R, Endris V, et al. Targeted next-generation sequencing enables reliable detection of HER2 (ERBB2) status in breast cancer and provides ancillary information of clinical relevance. *Genes Chromosomes Cancer*. 2017;56:255-265.
  21. von Minckwitz G, Kümmel S, Vogel P, et al. Neoadjuvant vinorelbine-capecitabine versus docetaxel-doxorubicin-cyclophosphamide in early nonresponsive breast cancer: phase III randomized GeparTrio trial. *J Natl Cancer Inst*. 2008;100:542-551.
  22. Goldhirsch A, Winer EP, Coates AS, et al. Personalizing the treatment of women with early breast cancer: highlights of the St Gallen international expert consensus on the primary therapy of early breast cancer 2013. *Ann Oncol*. 2013;24:2206-2223.
  23. Bustreo S, Osella-Abate S, Cassoni P, et al. Optimal Ki67 cut-off for luminal breast cancer prognostic evaluation: a large case series study with a long-term follow-up. *Breast Cancer Res Treat*. 2016;157:363-371.
  24. Holzschuh M-A, Czyz Z, Hauke S, Inwald EC, Polzer B, Brockhoff G. HER2 FISH results in breast cancers with increased CEN17 signals using alternative chromosome 17 probes: reclassifying cases in the equivocal category. *Histopathology*. 2017;71(4):610-625.
  25. Hudis CA, Barlow WE, Costantino JP, et al. Proposal for standardized definitions for efficacy end points in adjuvant breast cancer trials: the STEEP system. *J Clin Oncol*. 2007;25:2127-2132.
  26. Perrone G, Gaeta LM, Zagami M, et al. In situ identification of CD44+/CD24- cancer cells in primary human breast carcinomas. *PLoS One*. 2012;7:e43110.
  27. Mylona E, Giannopoulou I, Fasomytakis E, et al. The clinicopathologic and prognostic significance of CD44+/CD24(-/low) and CD44-/CD24+ tumor cells in invasive breast carcinomas. *Hum Pathol*. 2008;39:1096-1102.
  28. Rabinovich I, Sebastião APM, Lima RS, et al. Cancer stem cell markers ALDH1 and CD44+/CD24- phenotype and their prognosis impact in invasive ductal carcinoma. *Eur J Histochem*. 2018;62(24):2943-2950.
  29. Ricardo S, Vieira AF, Gerhard R, et al. Breast cancer stem cell markers CD44, CD24 and ALDH1: expression distribution within intrinsic molecular subtype. *J Clin Pathol*. 2011;64:937-946.
  30. Jaggupilli A, Elkord E. Significance of CD44 and CD24 as cancer stem cell markers: an enduring ambiguity. *Clin Dev Immunol*. 2012;2012:708036.
  31. Lehmann C, Jobs G, Thomas M, Burtscher H, Kubbies M. Established breast cancer stem cell markers do not correlate with in vivo tumorigenicity of tumor-initiating cells. *Int J Oncol*. 2012;41:1932-1942.
  32. Huber S, Wege AK, Bernhardt G, Buschauer A, Brockhoff G. Topotecan-induced ABCG2 expression in MCF-7 cells is associated with decreased CD24 and EpCAM expression and a loss of tumorigenicity. *Cytometry A*. 2015;87:707-716.
  33. Whittle JR, Lewis MT, Lindeman GJ, Visvader JE. Patient-derived xenograft models of breast cancer and their predictive power. *Breast Cancer Res*. 2015;17:17.
  34. Klein CA. Parallel progression of primary tumours and metastases. *Nat Rev Cancer*. 2009;9:302-312.
  35. Klein CA, Blankenstein TJF, Schmidt-Kittler O, et al. Genetic heterogeneity of single disseminated tumour cells in minimal residual cancer. *Lancet*. 2002;360:683-689.
  36. Vilgelm AE, Pawlikowski JS, Liu Y, et al. Mdm2 and aurora kinase a inhibitors synergize to block melanoma growth by driving apoptosis and immune clearance of tumor cells. *Cancer Res*. 2015;75:181-193.
  37. Fang DD, Tang Q, Kong Y, et al. MDM2 inhibitor APG-115 synergizes with PD-1 blockade through enhancing antitumor immunity in the tumor microenvironment. *J Immunother Cancer*. 2019;7:327.
  38. Zou Q, Jin J, Hu H, et al. USP15 stabilizes MDM2 to mediate cancer-cell survival and inhibit antitumor T cell responses. *Nat Immunol*. 2014;15:562-570.
  39. Haupt S, Vijayakumaran R, Miranda PJ, Burgess A, Lim E, Haupt Y. The role of MDM2 and MDM4 in breast cancer development and prevention. *J Mol Cell Biol*. 2017;9:53-61.
  40. Merkel O, Taylor N, Prutsch N, et al. When the guardian sleeps: reactivation of the p53 pathway in cancer. *Mutat Res*. 2017;773:1-13.
  41. Momand J, Jung D, Wilczynski S, Niland J. The MDM2 gene amplification database. *Nucleic Acids Res*. 1998;26:3453-3459.
  42. Karni-Schmidt O, Lokshin M, Prives C. The roles of MDM2 and MDMX in cancer. *Annu Rev Pathol*. 2016;11:617-644.
  43. Oliner JD, Saiki AY, Caenepeel S. The role of MDM2 amplification and overexpression in tumorigenesis. *Cold Spring Harb Perspect Med*. 2016;6(6):1-15.
  44. Turbin DA, Cheang MCU, Bajdik CD, et al. MDM2 protein expression is a negative prognostic marker in breast carcinoma. *Mod Pathol*. 2006;19:69-74.
  45. He X-Y, Xiang C, Zhang C-X, et al. p53 in the myeloid lineage modulates an inflammatory microenvironment limiting initiation and invasion of intestinal tumors. *Cell Rep*. 2015;13:888-897.
  46. Wang HQ, Mulford IJ, Sharp F, et al. Inhibition of MDM2 promotes antitumor responses in p53 wild-type cancer cells through their interaction with the immune and stromal microenvironment. *Cancer Res*. 2021;81:3079-3091.



47. Taylor A, Lee D, Allard M, Poland B, Greg SJ. Phase 1 concentration-QTc and cardiac safety analysis of the MDM2 antagonist KRT-232 in patients with advanced solid tumors, multiple myeloma, or acute myeloid leukemia. *Clin Pharmacol Drug Dev.* 2021;10:918-926.
48. Portman N, Milioli HH, Alexandrou S, et al. MDM2 inhibition in combination with endocrine therapy and CDK4/6 inhibition for the treatment of ER-positive breast cancer. *Breast Cancer Res.* 2020;22:87.
49. Saji S, Okumura N, Eguchi H, et al. MDM2 enhances the function of estrogen receptor alpha in human breast cancer cells. *Biochem Biophys Res Commun.* 2001;281:259-265.
50. Burgess A, Chia KM, Haupt S, Thomas D, Haupt Y, Lim E. Clinical overview of MDM2/X-targeted therapies. *Front Oncol.* 2016;6:7.
51. Al-Kuraya K, Schraml P, Torhorst J, et al. Prognostic relevance of gene amplifications and coamplifications in breast cancer. *Cancer Res.* 2004;64:8534-8540.
52. Fallahpour S, Navaneelan T, De P, Borgo A. Breast cancer survival by molecular subtype: a population-based analysis of cancer registry data. *CMAJ Open.* 2017;5:E734-E739.
53. Park HS, Park JM, Park S, Cho J, Kim SI, Park B-W. Subcellular localization of Mdm2 expression and prognosis of breast cancer. *Int J Clin Oncol.* 2014;19:842-851.
54. Minckwitz G von, Kaufmann M, Kuemmel S, et al. Correlation of various pathologic complete response (pCR) definitions with long-term outcome and the prognostic value of pCR in various breast cancer subtypes: results from the German neoadjuvant meta-analysis. *J Clin Oncol.* 2011;29:1028.

#### SUPPORTING INFORMATION

Additional supporting information may be found in the online version of the article at the publisher's website.

**How to cite this article:** Wege AK, Rom-Jurek E-M, Jank P, et al. *mdm2* gene amplification is associated with luminal breast cancer progression in humanized PDX mice and a worse outcome of estrogen receptor positive disease. *Int. J. Cancer.* 2022;150(8):1357-1372. doi:10.1002/ijc.33911